Acta Oceanol. Sin., 2023, Vol. 42, No. 5, P. 93–101
https://doi.org/10.1007/s13131-022-2121-2
http://www.aosocean.com
E-mail: ocean2@hyxb.org.cn

Mineralogy and geochemistry of hydrothermal sulphide from a submarine volcanic high at 18°36.4′S Central Lau Spreading Center, Southwest Pacific

Durbar Ray[1]*, Anil L. Paropkari[2]

[1] CSIR-National Institute of Oceanography, Dona Paula, Goa 403004, India

[2] Retired Chief Scientist, CSIR-National Institute of Oceanography, Goa 403004, India

Received 2 May 2022; accepted 20 September 2022

Abstract

We report the mineralogy and geochemistry of hydrothermal sulphide from the crater of a volcanic high near 18°36.4′S of the Central Lau Spreading Center. During 1990s, that volcanic structure was reported active and sulphide samples were collected by MIR submersible. A section of a chimney-like structure from the crater-floor was studied here. The Fe-depleted sphalerites, and Co-depleted pyrites in that chimney were similar to those commonly found in low to moderate temperature (<300℃) sulphides from sediment-starved hydrothermal systems. Bulk analyses of three parts of that chimney section showed substantial enrichment of Zn (18%–20%) and Fe (14%–27%) but depletion of Cu (0.8%–1.3%). In chondrite-normalized rare earth element-patterns, the significant negative Ce-anomalies (Ce/Ce*=0.27–0.39) and weakly positive Eu-anomalies (Eu/Eu*=1.60–1.68) suggested sulphide mineralisation took place from reduced low-temperature fluid. The depleted concentration of lithophiles in this sulphide indicates restricted contribution of sub-ducting plate in genesis of source fluid as compared to those from other parts of Lau Spreading Centre. Uniform mineralogy and bulk composition of subsamples across the chimney section suggests barely any alteration of fluid composition and/or mode of mineralisation occurred during its growth.

Key words: Central Lau Spreading Center, hydrothermal sulphide, mineralogy, geochemistry

Citation: Ray Durbar, Paropkari Anil L.. 2023. Mineralogy and geochemistry of hydrothermal sulphide from a submarine volcanic high at 18°36.4′S Central Lau Spreading Center, Southwest Pacific. Acta Oceanologica Sinica, 42(5): 93–101, doi: 10.1007/s13131-022-2121-2

1 Introduction

The western boundary of the Pacific Ocean has several actively spreading marginal basins or troughs (e.g., Lau, Woodlark, Manus, Fiji, Mariana, Okinawa, Izu-bonin, etc.); known for submarine hydrothermal activities and related mineral deposits (Fouquet et al., 1991; Bendel et al., 1993; Lisitzin et al., 1997; Glasby et al., 2000; Glasby and Notsu, 2003; Embley et al., 2004, Paropkari et al., 2010; Ray et al., 2014, 2017, 2018). Among these semi-isolated oceanic basins, the Lau Basin has relatively young back-arc setting and is characterised with number of active hydrothermal fields along its spreading centres and volcanic arcs. Till date, many sites of hydrothermal mineralisation have located at several parts of the Lau Basin. Earlier several studies described the geochemistry of hydrothermal deposits from the Valu Fa Ridge (VFR), Eastern Lau Spreading Center (ELSC), Tonga Volcanic Arc (TVA), Kings Triple Junction (KTJ) in this basin (Fouquet et al., 1991; Stoffers et al., 2006; Kim et al., 2009; Paropkari et al., 2010). In the Central Lau Spreading Center (CLSC), the evidence of seafloor hydrothermal activities was reported for the first time in the early 1990s (Malahoff and Falloon, 1991); however, no studies have addressed the geochemical features of hydrothermal sulphides from this segment of the Lau Spreading Center.

In the present study, the polymetallic sulphide deposit from a volcanic high within the CLSC has been investigated for mineralogy, mineral chemistry, and bulk elemental composition. Thus based on geochemical evidences, certain issues related to sulphide mineralisation and the physiochemical nature of source fluid have been discussed. Those geochemical features of sulphide from CLSC has also compared with hydrothermal sulphides of other segments of the Lau sPreading Center in light of the spatial variability in genesis of source fluid.

2 Local geological settings

In the Southwest Pacific, at the east of Fiji Island, the Lau Basin is a shallow trapezoidal-shaped marginal basin located near the convergent boundary of the Pacific and Indo-Australian plates (Fig. 1a). This basin was evolved through subduction of the Pacific plate and due to active spreading of the basin along the spreading axes over the past 6.0 Ma (Hawkins, 1995). An earlier study demonstrated that the Lau back-arc basin is composed of typical oceanic crust and characterized with high heat flow (Karig, 1970). Several actively spreading centres (e.g., VFR, ELSC, CLSC, Fonualei, Fotuna, Northeast and Northwest Lau Spreading centers) within this intra-oceanic basin (Zellmer and Taylor, 2001) might be the major sources for heat flux. Among those spreading axes, about 200 km long CLSC between 18°S and 19°25′S (Fig. 1b) is located more than 350 km away from the Tonga arc-trench system and flanked by elongated basins covered with thin sediment layer. Previous studies indicated that over the last 1.5 Ma, CLSC is propagating southward at the expense of the ELSC in the further south (Parson et al., 1990). However, it is also evident that the spreading rate of CLSC (87–

*Corresponding author, E-mail: dray@nio.org

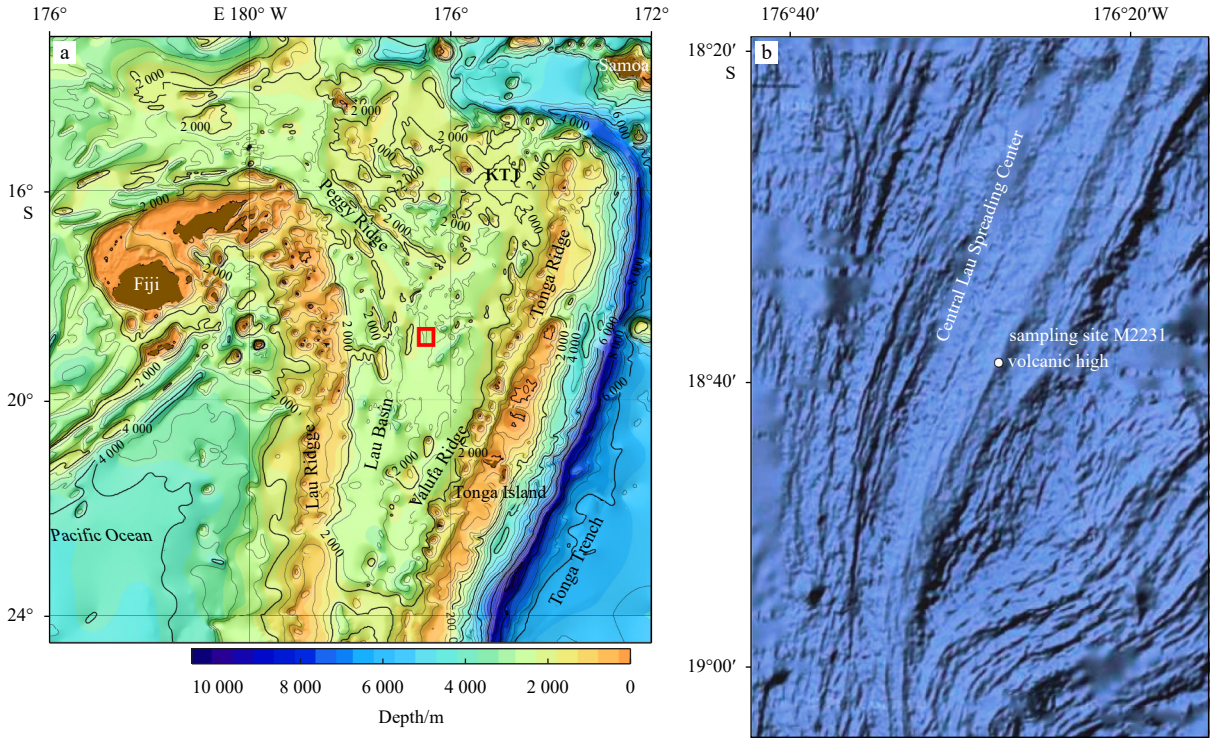

Fig. 1. Location of sulphide sampling site. a. Seafloor topography of the Lau Basin in the Southwest Pacific Ocean (modified after Paropkari et al. (2010)). The red box at the central part of the basin marks the location of the MIR diving site, A3 (dive No. M2231). b. The seafloor image of the Central Lau Spreading Center, displaying the sampling site over the volcanic high within the valley of the spreading axis. KTJ: Kings Triple Junction.

90 mm/a; Mottl et al., 2011) differs from relatively slow-spreading (39–61 mm/a) southern segments of that spreading centres (i.e., ELSC and VRF). The rocks from CLSC lies within the compositional range of typical N-MORB (Falloon et al., 1992; Pearce et al., 1994) and differs from typical arc-basalt, basaltic andesite, and rhyolite, found in other parts of the Lau spreading axis.

3 Sampling and analytical methodologies

In 1990–1991, during the multinational SUPACLARK (The Soviet Union-Papua New Guinea-Australia-Canada) and South Pacific Applied Geosciences Commission cruises on-board *ORV Akademik Mstislav Keldysh*, several marginal basins in the western Pacific were explored for hydrothermal activities and associated mineral deposits. During one of those cruises (April–June, 1990), hydrothermal fluid, sediment, rocks, mineral deposits, and seafloor photographs were collected with Russian deep water submersibles (i.e., *MIR-I* and *MIR-II*) from different parts of the Lau Basin. One of those MIR dives (No. M2231) was undertaken between 18°36.43′S and 18°37.35′S (site A3, Fig. 1a) to explore the possible hydrothermal activities within the valley of CLSC (Malahoff and Falloon, 1991). During that MIR dive, at the water depth between 2 242 m and 2 433 m, about 65 km^2 area of the valley floor were surveyed and later Falloon et al. (1992) described that diving site as the part of spreading axes of the constructional and active volcanic stage. An elongated volcanic high with partly collapsed caldera on its summit was located at the central part of the spreading center, near 18°36′S (Fig. 1b). Around that volcanic structure a variety of non-vesicular pillow, lobate, and sheet-types lava flows were observed (Falloon et al., 1992). The evidences of active venting and associated sulphide deposits were also reported inside the crater of that volcanic high (Malahoff and Falloon, 1991). From that crater floor (at 18°36.42′S, 176°26.6′W) mostly basaltic rocks, lava, and hydrothermal sulphides were sampled. One of those sulphide samples (M2231-10, Fig. 2a) collected from the water depth of 2 248 m; was used for the present geochemical investigation.

3.1 *Sample description*

The hand specimen of the sulphide sample, M2231-10, was mostly brownish-orange in colour, and have some black patches on it (Fig. 2a). It has a dark central groove, and which appeared as a clogged fluid orifice (Fig. 2b). Usually such colour variations within individual hydrothermal structure represents multiple mineral zonings; evolved through multiple phases of mineralisation (Koski et al., 1994; Paropkari et al., 2010; Sun et al., 2012; Ray et al., 2018). Therefore, with an aim to study the possible geo-

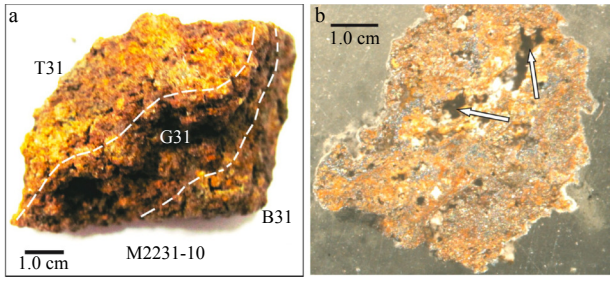

Fig. 2. The sulphide deposit, M2231-10 from Central Lau Spreading Center, Lau Basin. a. The sulphide was sub-sampled into three sections, T31, G31 and B31; as marked by white lines. b. The cross-sectional view of the sub-sample G31, shows the openings of fluid channels (marked by the arrows).

chemical variations within this sulphide deposit, three sub-samples having minor colour differences (Fig. 2a) were separated carefully. Thus the top yellowish-orange part (T31), the black central groove (G31), and the brownish bottom portion (B31) were separately analysed for mineralogy, mineral chemistry and bulk composition.

3.2 *Mineralogy of sulphides*

After separation, all three sub-samples were cleaned with water, and then dried at room temperature. A part of each sub-sample was powdered with an agate-mortar and analysed for mineralogical composition by using a Xray-diffractometer (XRD) (Model: Rigaku-Ultima-IV). Each sample was scanned thoroughly by using Cu-Kα radiation over the 2θ ranging from 2° to 60°. Minerals were identified with RIGAKU peak-search software and JCPDS database. To examine the micro-texture of minerals, several minute pieces were randomly picked-up from each sub-sample and scanned with a Scanning Electron Microscope (Model: JEOL JSM-5410LV).

3.3 *Mineral chemistry of sulphides*

Different minerals of this sulphide deposit were analysed for chemical composition with an Electron Probe Micro Analyser (EPMA) equipped with four wavelength-dispersive spectrometers. For that, small pieces of each sub-sample were mounted on resin and polished thoroughly. The elemental composition of minerals was analysed by using an accelerating voltage of ~15 kV, the beam current and beam diameter of ~12 nA, and 2.0 μm, respectively. The standard minerals of pyrite, and sphalerite (from SPI Supplies, West Chester, PA, USA) were used to assess the accuracy of instrumental analyses.

3.4 *Bulk composition of chimney sulphide*

Three sub-samples were separately analysed for bulk composition. Fifty milligrams of dry finely powdered samples were mixed with 10 mL ultra-pure acid mixture ($HF:HNO_3:HClO_4$=7:3:1) in Teflon beakers and then evaporated to dryness on a hot-plate at ~150℃. To this digested residue, 20 mL ultra-pure (1:1) HNO_3 was added and then diluted up to 250 mL with Milli-Q® water. In these diluted solutions, the concentration of major elements like Fe, Cu, Mn, and Zn were determined with Flame-AAS (Model: Perkin Elmer, Analyst-200) using SCO-1, SGR-1 as reference standards. The trace element and rare earth element (REE) concentrations were measured with a quadrupole ICP-MS (Model: Perkin Elmer SCIEX ELAN DRC-II) using 1.0 mL of ^{103}Rh solution (20 ng/mL) as internal standard. Analytical accuracy of ~ ±2.0% was achieved against the marine reference material, MAG-1 and the precisions were better than 4.0% RSD.

4 Results and discussion

4.1 *Physical features of hydrothermal sulphide from the volcanic high in CLSC*

The hand specimen of the sulphide sample, M2231-10 (Fig. 2a) has very rough and porous surface (Fig. 3a). Some parts of this sulphide had thin coating of orange-coloured Fe-oxides; indicating partial weathering of the sample. In microphotographs, the feathery appearance of that Fe-rich surface coating (Fig. 3b) also suggests the presence of amorphous Fe-oxides/oxy-hydroxides on the sample. Even though, this sulphide sample doesn't reveal typical columnar structure; but certain characters of this deposit particularly surface porosity and channel openings were very similar to any hydrothermal chimney or spire, rather than volcanogenic massive sulphide deposits. Earlier, Malahoff and Falloon (1991) have also described the same sulphide sample as part of an isolated chimney. At the middle part of this sulphide (i.e., sub-sample, G31), there were multiple cavities; appeared as fluid conduits (Fig. 2b). All these conduits were characterised with narrow irregular-shaped openings (Fig. 2b), which suggests, sluggish fluid-flow took place through those twisted channels. The SEM photographs of one of these channels showed the inner wall was smooth and characterised with fine cracks (Fig. 3c). In the cross-section of this chimney several scattered, dark patches were found; however, no distinct layers of concentric mineral zonings have been observed. Such physical features including multiple conduits, smaller edifice, and lack of mineral zonings of this sample resemble typical low-temperature hydrothermal chimneys described elsewhere (Koski et al., 1994).

4.2 *Mineralogical features of M2231-10 chimney*

The XRD analyses of sub-samples of this chimney section (M2231-10) showed it mainly composed of sphalerite and pyrite; with traces of marcasite and galena (Table 1). These metal-sulphides were found to associate with amorphous and opaline silica (Table 1; Fig. 4). The backscatter images also showed disseminated fine (size: 150 μm or less) pyrite and sphalerite grains are co-existing with silica in all three sub-samples of this chimney section (Fig. 4). In porous outer sub-samples (i.e., T31 and B31), the dendritic and colloform pyrite and sphalerite were found more (Figs 4a, b); which apparently indicates direct non-equilibrium precipitation of sulphide took place from fluids without re-crystallisation. While, relatively less porous, inner G31 sub-sample have more developed sulphide crystals; embedded in amorphous siliceous mass (Fig. 4c); suggesting the interspace of sulphide grains were filled-up by late-stage precipitation of silica. At the waning phase of chimney growth, probably cooling of the chimney caused silica-saturation in source fluid and that might deposit the colloform silica as gangue minerals (Figs 4c, d) and thus apparently marked separate paragenetic regimes for this chimney development.

The major minerals (i.e., pyrite, sphalerite, and opal) from three sub-samples were analysed for chemical composition and the results obtained from microprobe analyses are presented in Table 2. Analyses of sphalerites showed the range of composition with 52.9–59.4 wt% of Zn, 3.0–4.5 wt% of Fe, and 32.6–33.9 wt% of S (Table 2); representing the average composition of $Zn_{0.83}Fe_{0.06}S_{1.04}$. The inclusion of Fe in lattice structure of hydrothermal sphalerite is quite common and that occurs through partial replacement of Zn^{2+} with Fe^{2+}. Usually degree of such elemental substitution depends on the mineralisation temperature and geochemical nature of source fluid (Scott, 1983). Several evidences showed that sphalerite with higher Fe-content occurs in high-temperature hydrothermal deposits, while Fe-poor sphalerite are reported in relatively low-temperature (<300℃) Zn-rich sulphides (Koski et al., 1994; Wang et al., 2017b; Lehrmann et al., 2018). The Fe/Zn ratio in sphalerite crystal which indicate the relative enrichment of Fe, were ranged between 0.051 and 0.085 (av. Fe/Zn=0.067±0.01) in the M2231-10 chimney sample. These estimated Fe/Zn ratios were very similar to Fe-depleted sphalerite (Fe/Zn<0.2), reported in many other sediment-starved hydrothermal systems (e.g., Vai-Lili, Trans-Atlantic Geotraverse (TAG), Meso zone, PACMANUS, Kairei) characterized with fluids having higher fugacity of sulphur (fs_2) and oxygen (fo_2) (Keith et al., 2014). It has also proposed that in such sediment-starved hydrothermal deposit, the Fe-concentration in sphalerite is the function of fluid temperature ($Fe/Zn_{sphalerite}$= 0.001 3T–0.295 3; Keith

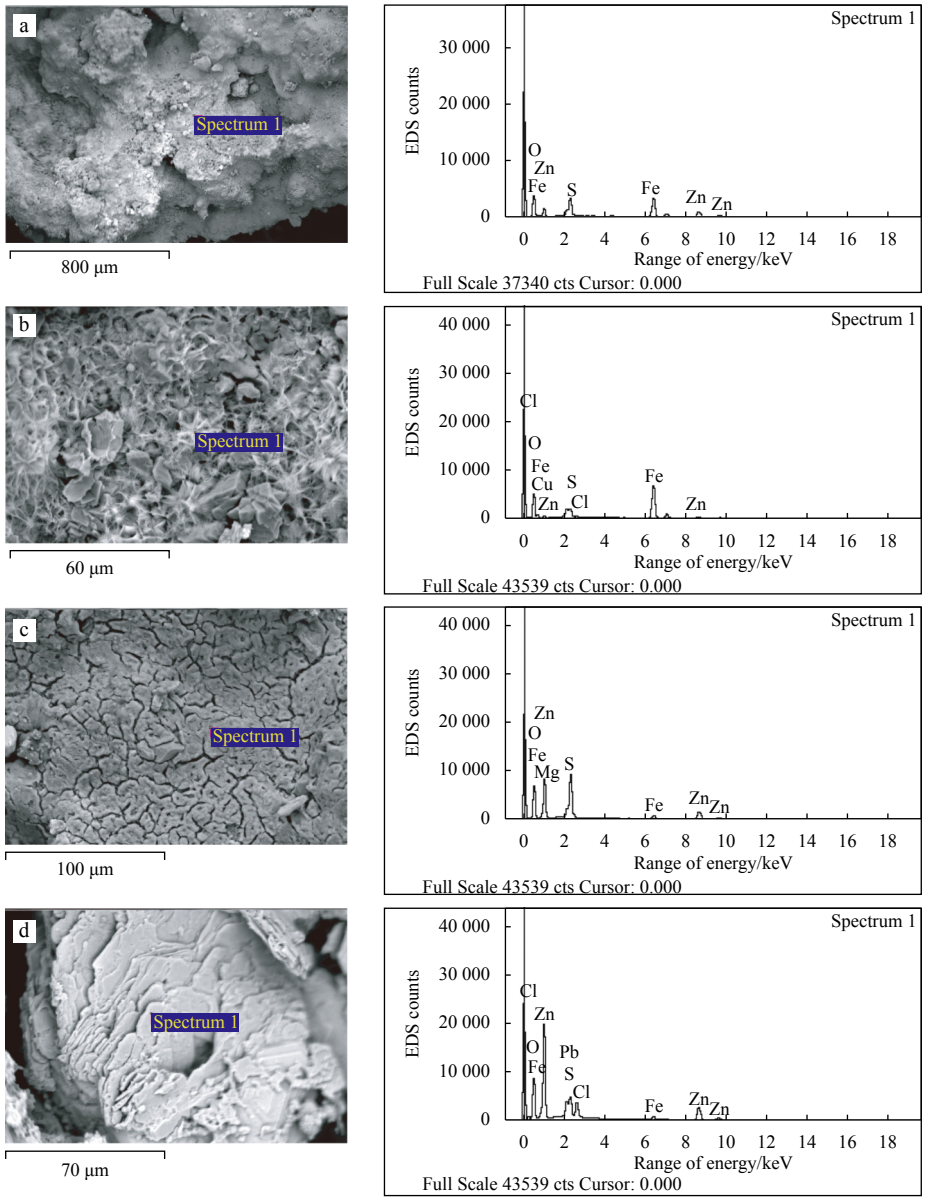

Fig. 3. Scanning electron microscope photographs and corresponding enegy dispersive X-ray spectroscopy (EDS) results of the surface of hydrothermal sulphide (M2231-10) from volcanic high at Central Lau Spreading Center (a); the magnified image of Fe-rich coating on B31 section (b); the inner surface of fluid channel in G31 section (c), and anhedral Zn-sulphide deposits in T31 section (d).

Table 1. Mineralogical composition of three sections in hydrothermal sulphide sample, M2231-10 from the crater-floor of the volcanic high at Central Lau Spreading Center, Lau Basin

	Top layer (T31)	Middle layer around the central groove (G31)	Bottom layer (B31)
Major minerals	sphalerite, opaline silica	sphalerite, pyrite, opaline silica	pyrite, sphalerite
Trace minerals	pyrite, galena	marcasite	galena, opaline silica

et al., 2014). Considering the same relation, the estimated $Fe/Zn_{sphalerite}$ ratios (i.e., 0.051 to 0.085) of the present study indicates the sphalerite mineralization temperature in the M2231-10 sulphide sample had a range of 266–287℃ with an average value of 278℃. This range of mineralisation temperature was very similar to those reported for non-recrystallized sphalerite formed at low to moderate-temperature (230–<300℃) zones of the TAG hydrothermal mound (Lehrmann et al., 2018). Among other trace elements, Cd has considerably elevated concentrations (0.2%–0.6%, Table 2) in this sphalerite and that could be due to the substitution of Zn^{2+} by the Cd^{2+} within the sphalerite lattice. In some cases, traces of Cu, Ni, and Co have also been detected in these sphalerite crystals, ranges between below detection to 0.06 wt%; Table 2).

Another abundant sulphide mineral, pyrite in this chimney showed a range of composition with Fe and S concentrations of 45.1–49.5 wt% and 49.5–54.6 wt%, respectively (Table 2), and which corresponds an average composition of $Fe_{1.0}S_{2.19}$. Generally hydrothermal pyrite develops over wide range of temperature and thus the relative abundance of S and Fe may alter accordingly. Studies showed that the S/Fe ratios in hydrothermal pyrite are usually controlled by formation conditions and have a

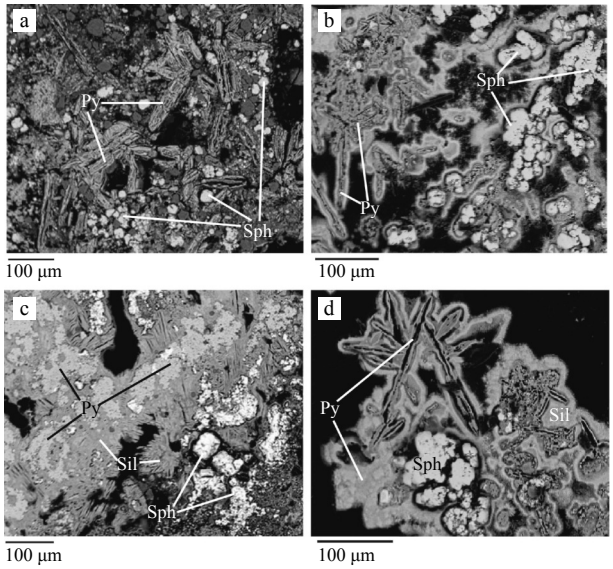

Fig. 4. Back-scatter electrons microphotographs (obtained from EPMA) of mineral assemblages in polished sections of the layers, T31, and B31 of sulphide deposit, M2231-10. a. Sphalerite (white) and pyrite (light grey) embedded in silica (dark grey) in B31; b. colloform silica (grey) layered to concentric pyrite (off white) and sphalerite (white) in T31; c. pyrite embedded in amorphous silica in B31; d. pyrite and sphalerite in G31 section.

negative relation with crystallisation temperature (Zhang et al., 2018 and references therein). The estimated average S/Fe ratio (~2.2) in pyrites of M2231-10 chimney section was relatively high and comparable to typical low-temperature hydrothermal pyrites (S/Fe >2.0; Zhang et al., 2018). Thus in this chimney sample, the dendritic and colloform pyrites which commonly develops through rapid non-equilibrium precipitation might represents the second generation of low temperature (100–250℃) sulphide mineralisation. In hydrothermal pyrites, the incorporation of elements like Cu, Co, Ni usually occurs as the solid solution; and which have significantly low concentrations (<0.03 wt%, Table 2) in this sample. This also could be due to limited isomorphic elemental substitutions within pyrite crystals at lower temperature. Earlier several studies indicated that enhanced partitioning of Co into pyrite occurs at high temperature (>300℃) and reduced conditions (Grant et al., 2018; Maslennikov et al., 2020; Meng et al., 2020). Therefore, depleted Co contents also indicate pyrite mineralization in the M2231-10 chimney took place at reduced temperature. Another common lattice bound element, Ni also shows depleted concentration in this sample, resulting the Co/Ni ratios close to unity and were substantially lower than those documented in typical high-temperature hydrothermal sulphides (Co/Ni≫1.0; Keith et al., 2016; Maslennikov et al., 2017).

The microprobe analyses of a number of siliceous infills within the interspaces of sulphide crystals in T31 and G31 subsamples showed consistent composition having ~46 wt% and ~53 wt% of Si and O, respectively (Table 2); and which corresponds to the atomic ratio close to pure silica. However, the amorphous silica in this sulphide structure has also found with Al (<0.3%) and Fe (<0.5%) (Table 2) and which could present as traces of metallic-silicates and/or the impurities within the siliceous deposit.

4.3 *Bulk geochemistry of M2231-10 chimney sulphide*

4.3.1 *Major and trace element composition*

In M2231-10 chimney sulphide, the bulk concentrations of major ore-forming elements including Cu, Zn, and Fe were varied between the ranges of 0.8%–1.3%; 18.1%–20.4% and 14.5%–26.9%, respectively (Table 3). Even though the mobility of Cu in hydrothermal fluid and therefore, Cu-mineralisation primarily depends on fluid temperature; but the estimated Cu contents in this chimney were considerably higher than those (Cu<0.5%) in

Table 2. The elemental composition of major minerals (e.g., pyrite, sphalerite, and opaline silica) in three sub-samples of hydrothermal sulphide, M2231-10 from the volcanic high at Central Lau Spreading Center, Lau Basin. The below detection limit (bdl) of microprobe analyses corresponds to the concentration <0.01%

Sample	Pyrite								
	Fe/%	Co/%	Ni/%	Cu/%	Zn/%	Si/%	S/%	Cd/%	Total/%
T31	47.79	0.02	0.01	0.02	0.01	0.06	52.44	bdl	100.4
	49.50	0.01	0.01	0.02	0.04	1.21	49.51	bdl	100.3
	45.14	0.03	0.02	0.02	0.01	0.09	54.59	bdl	99.9
	46.59	bdl	bdl	0.03	bdl	0.05	53.86	bdl	100.5
	47.30	0.02	bdl	bdl	bdl	0.02	53.42	bdl	100.8
	47.13	bdl	bdl	bdl	0.04	0.02	53.52	bdl	100.7
Sample	Sphalerite								
	Fe/%	Co/%	Ni/%	Cu/%	Zn/%	Si/%	S/%	Cd/%	Total/%
T31	4.54	0.02	0.06	0.03	53.11	0.13	33.92	0.41	92.2
	3.65	0.02	0.06	0.04	55.47	0.02	33.76	0.21	93.2
	3.62	bdl	0.02	0.01	52.94	1.35	32.66	0.42	91.0
	3.04	bdl	0.05	bdl	59.45	0.49	33.39	0.59	97.0
Sample	Opaline silica								
	Al/%	Fe/%	Co/%	Cu/%	Zn/%	Si/%	S/%	O/%	Total/%
T31	0.03	0.33	bdl	bdl	0.01	46.66	0.13	53.28	100.4
	0.14	0.38	0.01	bdl	0.08	46.51	0.14	53.22	100.5
G31	0.29	0.51	bdl	bdl	0.04	46.01	0.18	53.05	100.1
	0.30	0.35	0.02	bdl	0.09	46.24	0.13	53.14	100.3
	0.08	0.31	0.02	bdl	0.07	46.55	0.21	53.26	100.5

Table 3. The concentration of major and trace elements in three sub-samples of hydrothermal sulphide (M2231-10) from volcanic high at Central Lau Spreading Center (CLSC), Lau Basin

Elements	Sections of hydrothermal sulphide from CLSC (M2231-10)		
	T31	G31	B31
	Major elements/wt%		
Mn	0.08	0.08	0.10
Fe	14.50	20.10	26.90
Cu	1.32	1.01	0.88
Zn	20.40	19.60	18.10
Cu+Zn	21.70	20.60	19.90
Cu/Zn	0.06	0.05	0.10
	Trace elements/10^{-6}		
Sc	12.13	13.74	13.30
Ti	89.90	93.41	85.14
V	66.24	69.55	71.30
Ni	0.91	0.95	1.59
Rb	4.94	4.87	4.12
Sr	2.06	2.17	2.05
Y	0.26	0.17	0.31
Zr	4.77	5.51	4.65
Nb	0.38	0.40	0.41
Mo	13.87	14.56	17.15
Cd	1 319	1 230	856
Sn	20.12	19.51	20.98
Ba	27.68	29.07	34.86
Hf	0.11	0.23	0.22
W	1.59	1.13	1.07
Pb	906	1 029	1 082
Th	0.062	0.091	0.060
U	0.11	0.078	0.097
Ba/Nb	72.70	72.60	85.00

typical low-temperature (<300℃) Zn or Fe-rich sulphides described in several earlier studies (Koski et al., 1994; Wang et al., 2017a). However, relative to bulk Zn concentrations, these Cu contents were quite less, and that results low Cu to Zn ratio (Cu/Zn=0.05–0.1, Table 3); which resembles many low to moderate temperature hydrothermal sulphides (James and Elderfield, 1996; Paropkari et al., 2010; Ray et al., 2018). Besides the temperature of formation, the nature of source rock also controls the metal contents in end-member fluid and thus, in sulphide deposits (Wohlgemuth-Ueberwasser et al., 2015). In Fig. 5, the plot of Cu/Zn ratios against the cumulative concentrations of Cu and Zn indicates the fluid responsible for this volcanic deposit in CLSC is apparently originated through reactions of seawater with basalts rather than ultramafic rocks. Furthermore, the concentrations of Mn (0.08%–0.1%, Table 3) in this chimney were considerably higher than those reported in typical high temperature sulphides and resemble low temperature formations (Koski et al., 1994; Paropkari et al., 2010). Earlier studies indicated that at lower temperatures, vapour-rich less saline fluid favours Mn enrichment in hydrothermal deposit (Suzuki et al., 2008; James et al., 2014). In the present study, no Mn-bearing minerals have been identified; and therefore, the elevated concentration of Mn might also be results from micro-inclusions of Mn through the adsorption on colloform sulphides.

The trace elements having higher mobility in hyper-saline, high-temperature fluid did not show notable enrichments (e.g., Mo: 13×10^{-6}–17×10^{-6}, Sn: 19×10^{-6}–21×10^{-6}, and W: 1×10^{-6}–1.5×10^{-6}; Table 3); in M2231-10 chimney, as compared to those found

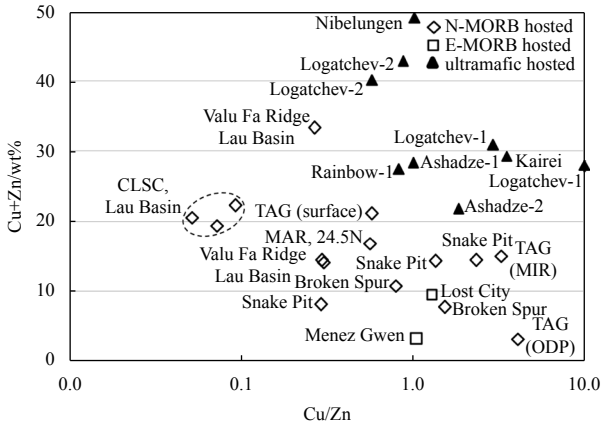

Fig. 5. Comparison of cumulative concentration of Cu and Zn in relation to Cu/Zn ratios in hydrothermal sulphides from basalt and ultramafic hosted fields (modified after Fouquet et al. (2010)). CLSC: Central Lau Spreading Center; TAG: Trans-Atlantic Geotraverse; MAR: Mid-Atlantic Ridge; ODP: Ocean Drilling Program.

in high temperature sulphides (Münch et al., 1999; Wang et al., 2017a) and thus also confirm its low temperature formation. In contrast, this sphalerite-pyrite-rich chimney was characterised with elevated concentrations of Cd (856×10^{-6}–$1\,319\times10^{-6}$) and Pb (906×10^{-6}–$1\,082\times10^{-6}$) (Table 3). Previous studies on Zn-rich low to moderate-temperature hydrothermal deposits also showed the abundances of Pb, and Cd have positive relations with Zn-enrichment (Münch et al., 2001). Such coherent behaviour of these elements in hydrothermal sulphide is possibly due to similar solubility of stable complexes of Zn, Cd, and Pb in low-temperature, less saline fluid. In addition to that, the cationic substitution of Zn^{2+} with Pb^{2+} or Cd^{2+} within the sphalerite lattice (Tivey, 1995) and the tendency of Pb^{2+}, Cd^{2+} and Zn^{2+} ions to get adsorbed on colloform Fe-sulphides (Grant et al., 2018) may also likely responsible for such Cd and Pb enrichments.

This M2231-10 chimney section showed the concentrations of lithophilic elements like Ba and Rb in the range of 27×10^{-6}–34×10^{-6} and 4.1×10^{-6}–4.9×10^{-6} respectively (Table 3). As compared to usual low temperature sphalerite/pyrite rich chimneys (Ba=40×10^{-6}–$10\,000\times10^{-6}$; Koski et al., 1994) this estimated ranges of lithophiles were substantially less. Moreover, such low accretion of lithophiles is also contrasting to the hydrothermal sulphides reported over the Lau spreading axes in further south; which are heavily enriched in Ba (e.g., 2.6×10^{-6}–0.25 Ba in ELSC; 2%–20% Ba in VFR) (Fouquet et al., 1991; Sun et al., 2012; Evans et al., 2017). The reason for such order of differences in Ba content among these hydrothermal sulphides (Fig. 6) is not very clear; but the effects of sub-seafloor processes for depleted Ba in CLSC sulphide cannot be ruled out. In back-arcs, the depleted contribution from subducting plate might cause less lithophiles in hydrothermal fluid and minerals. According to the model-based study of Perrin et al., (2018); it is evident that the larger volume of mantle wedge would restrict the contribution sub-ducting plate below CLSC as compared to the southern segments of Lau spreading axes (i.e., ELSC and VFR), closer to the subduction zone. Based on rocks geochemistry, Pearce et al. (1994) also demonstrated that the inputs of subduction in melt genesis systematically reduced from VFR to ELSC followed by CLSC as their distance from the arc increases towards the north. Therefore, even this study has limited analytical results; but the depleted Ba in CLSC sulphide suggests restricted supply of lithophiles from subducting plate in source

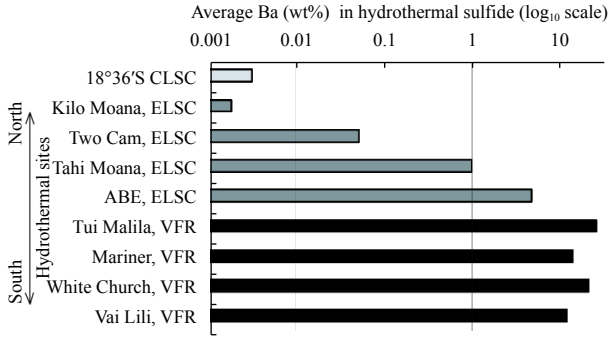

Fig. 6. Spatial distribution of average Ba concentrations (wt%) of hydrothermal sulphides from vent fields along different spreading centres of the Lau Basin. The Ba contents in sulphides of Eastern Lau Spreading Center (ELSC) and Valu Fa Ridge (VFR) are obtained from Fouquet et al. (1991), Sun et al. (2012), and Evans et al. (2017).

fluid. The high field strength elements (HFSEs) which behave conservatively during subduction-induced magmatic processes; have considerable abundances (e.g., Zr=4.6×10^{-6}–5.5×10^{-6}, Nb=0.38×10^{-6}–0.41×10^{-6}, Hf=0.1×10^{-6}–0.23×10^{-6}; Table 3) in this chimney sulphide. Thus, lithophile to HFSE ratio; another prominent indicator for the contribution of sub-ducting plate in melt generation, was not very high (e.g., Ba/Nb<85; Table 3); also suggesting reduced contribution of subducting plate in hydrothermal fluid genesis.

4.3.2 *Rare earth element systematics*

Like other trace elements, the geochemistry of rare earths in hydrothermal sulphides also carries many significant evidences for evolutionary processes; as the sulphides inherit most of the characteristic REE-features from the source fluid. The total REE content (∑REE) in three sub-samples of M2231-10 chimney vary between 1.103×10^{-6}–1.33×10^{-6} (Table 4). These total REE contents were slightly more than the values (∑REE=0.17×10^{-6}–1.12×10^{-6}) reported in several other low-temperature sphalerite-rich hydrothermal sulphides (Hongo and Nozaki, 2001; Paropkari et al., 2010; Zeng et al., 2015). Considerable presence of colloform Fe-sulphide would probably responsible for accretion of more REEs in M2231-10 chimney. Despite the variable ranges of total REE; the chondrite (C1)-normalized REE-patterns of CLSC chimney section have very similar trends of hydrothermal sulphides from other marginal basins (Fig. 7). All three REE patterns of subsamples from M2231-10 chimney were characterised with LREE-HREE fractionation, positive Eu and negative Ce anomalies. Result shows, the lighter REEs (LREE, e.g., La, Ce, Pr, Nd, Sm, and Eu) represents the major fraction of the REE contents (i.e., >84% of ∑REE) in this CLSC sulphide. The relative LREE-HREE fractionation; which usually represents in terms of $(Nd/Yb)_{CN}$ ratios, also has values (=2.06–3.48; Table 4), similar to those reported in other Zn-rich sulphide deposits (Mills and Elderfield, 1995; Paropkari et al., 2010). Generally, REE fractionation in sulphides represents the imprint of parent fluid; which mostly developed due to higher mobility of LREEs as compared to heavier rare earths. This chimney from CLSC were characterised with very weak positive Eu-anomalies (Eu/Eu*=1.6–1.68; Table 4); and that suggests the factors for stability of dissolved Eu^{2+} ions in fluid particularly the temperature and salinity might be low. In low temperature source fluid, limited availability of complexing agents like F^-, Cl^-, SO_4^{2-} etc. for REEs might cause weak Eu-anomalies in this hydrothermal sulphide. Furthermore, the appearance of pronounced negative Ce-anomalies (Ce/Ce*=0.27–0.39; Table 4) in this silica-rich chimney sulphide samples are interesting. Usually, such negative Ce-anomaly in hydrothermal sulphides are considered as the imprints of seawater (Barrett et al., 1990). Therefore, the observed Ce-anomaly and enrichment of opaline silica in this hydrothermal sulphides indicates substantial convective mixing of seawater during hydrothermal precipitation. The geochemical characteristics of Y are very similar to Ho and thus due to comparable behaviour in various geochemical processes, these elements maintain characterized molar ratios. The estimated Y/Ho molar ratios in this sulphide have a range between 45 and 48.2; which were close to typical chondritic ratio (Y/Ho~52; Anders and Grevesse, 1989) but lower than the values

Table 4. The concentrations of rare earth elements (×10^{-6}) in three sub-samples of hydrothermal sulphide (M2231-10) collected from volcanic high at Central Lau Spreading Center (CLSC), Lau Basin

REEs	Sections of hydrothermal sulphide from CLSC (M223-10)		
	T31	G31	B31
La	0.348	0.285	0.385
Ce	0.358	0.284	0.256
Pr	0.055	0.051	0.057
Nd	0.218	0.205	0.270
Sm	0.068	0.046	0.059
Eu	0.081	0.070	0.071
Gd	0.062	0.044	0.038
Tb	0.010	0.007	0.008
Dy	0.046	0.036	0.039
Ho	0.010	0.007	0.012
Er	0.027	0.028	0.033
Tm	0.005	0.004	0.004
Yb	0.037	0.029	0.027
Lu	0.009	0.007	0.007
∑REE	1.334	1.103	1.265
$(Nd/Yb)_{CN}$	2.06	2.46	3.48
$(Eu/Eu^*)_{CN}$	1.61	1.68	1.60
$(Ce/Ce^*)_{CN}$	0.39	0.34	0.27
Y/Ho (molar)	48.2	45.0	47.9

Note: CN=chondrite normalized values (from Sun and McDonough (1989)); $(Eu/Eu^*)_{CN}=Eu_{CN}/(Sm_{CN}+Gd_{CN})^{0.5}$ and $(Ce/Ce^*)_{CN}=Ce_{CN}/(La_{CN}+Pr_{CN})^{0.5}$.

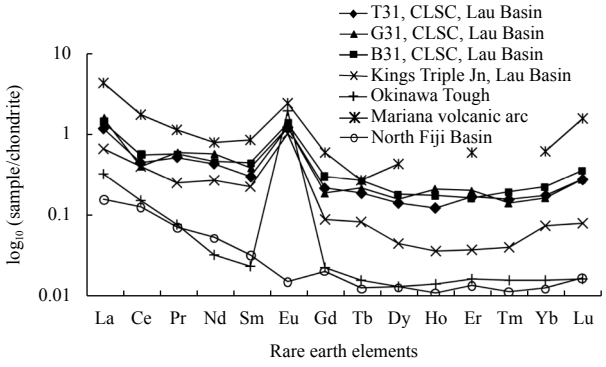

Fig. 7. Chondrite normalized REE-patterns of sub-samples from hydrothermal chimney, M2231-10. Those REE-patterns are compared with other sphalerite and pyrite-rich sulphides from Okinawa Trough (Hongo and Nozaki, 2001); Lau Basin (Paropkari et al., 2010); Mariana volcanic arc (Hein et al., 2014); Fiji Basin (Zeng et al., 2015) in the western Pacific.

reported in seawater (Y/Ho=67–102; Bau et al., 1997). A similar observation has been mentioned by Hongo and Nozaki (2001) in hydrothermal sulphides from the Okinawa Trough. This result suggests the end-member fluid might retain the characteristic Y to Ho fractionation of magma sources and even did not alter much prior to sulphide mineralization.

4.4 *Variations of mineralogy and elemental geochemistry within the chimney section*

The relative distribution of minerals across the chimney section showed that the brown subsample (B31) and the subsample around the central groove (G31) were relatively rich in Fe-sulphides; while the yellowish top portion (T31) contents more sphalerite (Fig. 2a). Similarly, the major element, particularly, the Fe contents was found to increase from light coloured T31 section to innermost G31 and bottom B31; while, the Zn concentrations have an opposite trend, which gradually depleted from T31 to G31 and B31 (Table 3). However, the bulk concentrations of Cu, Mn, and most of the other trace elements did not show any major variation across these chimney section (Table 3). Likewise, the REE patterns of the three sub-samples also closely resembled each other (Fig. 7). Usually, considerable changes in end-member fluid temperature and/or composition due to alteration of seawater to fluid mixing ratio causes substantial mineralogical and elemental variations within individual hydrothermal deposits (Dekov et al., 2015; Ray et al., 2018). Therefore, the minor differences of mineralogical, and elemental compositions within this sulphide structure suggest, besides the paragenetic shift from the sulphide phase to late stage silica phase, there were no significant changes in end-member fluid during the growth of this chimney.

5 Conclusions

Hydrothermal sulphide from a submarine volcanic crater in CLSC at 18°36′S were investigated for mineralogy, mineral chemistry and elemental geochemistry. The physical and geochemical features of that sulphide deposit were very similar to hydrothermal chimney rather than any massive volcanic deposit. Even though the nature of source fluid of this sulphide is not known, but the pieces of evidence from mineral-assemblages and their chemistry indicate this sulphide chimney formed at moderate temperature of ~278℃. Mineralogical evidences also indicate mineralisation temperature was dropped over the chimney growth and might be responsible for paragenetic shifts from subhedral to colloform sulphides and then to silica phase. The bulk elemental composition of this silicified hydrothermal sulphide suggests the genesis of end-member fluid involved typical sediment-free MORB-seawater reactions. However, the depleted contribution of the sub-ducting plate in melt genesis was made this polymetallic sulphide in CLSC more unique than those from southern segments of the Lau spreading center.

Acknowledgements

The authors are thankful to the Director, CSIR-NIO, Goa for providing necessary facilities for this study. Anil L. Paropkari is highly grateful to Alexander P. Lisitsyn for inviting him to participate in the cruise on-board R/V *Akademik Mstislav Keldysh* and sharing sulphide samples to undertake scientific investigation. Thanks to Prabhu and Khedekar for XRD and EPMA analyses, respectively. This manuscript has CSIR-NIO contribution No. 6976.

References

Anders E, Grevesse N. 1989. Abundances of the elements: meteoritic and solar. Geochimica et Cosmochimica Acta, 53(1): 197–214, doi: 10.1016/0016-7037(89)90286-X

Barrett T J, Jarvis I, Jarvis K E. 1990. Rare earth element geochemistry of massive sulfides-sulfates and gossans on the Southern Explorer Ridge. Geology, 18(7): 583–586, doi: 10.1130/0091-7613(1990)018<0583:REEGOM>2.3.CO;2

Bau M, Möller P, Dulski P. 1997. Yttrium and lanthanides in eastern Mediterranean seawater and their fractionation during redox-cycling. Marine Chemistry, 56(1–2): 123–131

Bendel V, Fouquet Y, Auzende J M, et al. 1993. The White Lady hydrothermal field, north Fiji Back-Arc Basin, Southwest Pacific. Economic Geology, 88(8): 2237–2245, doi: 10.2113/gsecongeo.88.8.2237

Dekov V M, Lalonde S V, Kamenov G D, et al. 2015. Geochemistry and mineralogy of a silica chimney from an inactive seafloor hydrothermal field (East Pacific Rise, 18°S). Chemical Geology, 415: 126–140, doi: 10.1016/j.chemgeo.2015.09.017

Embley R W, Baker E T, Chadwick Jr W W, et al. 2004. Explorations of Mariana arc volcanoes reveal new hydrothermal systems. EOS, Transactions American Geophysical Union, 85(4): 37–40

Evans G N, Tivey M K, Seewald J S, et al. 2017. Influences of the Tonga Subduction Zone on seafloor massive sulfide deposits along the Eastern Lau Spreading Center and Valu Fa Ridge. Geochimica et Cosmochimica Acta, 215: 214–246, doi: 10.1016/j.gca.2017.08.010

Falloon T J, Malahoff A, Zonenshain L P, et al. 1992. Petrology and Geochemistry of back-arc basin basalts from Lau Basin spreading ridges at 15°, 18° and 19°S. Mineralogy and Petrology, 47(1): 1–35, doi: 10.1007/BF01165295

Fouquet Y, Cambon P, Etoubleau J, et al. 2010. Geodiversity of hydrothermal processes along the Mid-Atlantic ridge and ultramafic-hosted mineralization: a new type of oceanic Cu-Zn-Co-Au volcanogenic massive sulfide deposit. In: Rona P A, Devey C W, Dyment J, et al., eds. Diversity of Hydrothermal Systems on Slow Spreading Ocean Ridges. Washington: American Geophysical Union, 321–367

Fouquet Y, von Stackelberg U, Charlou J L, et al. 1991. Hydrothermal activity in the Lau back-arc basin: sulfides and water chemistry. Geology, 19(4): 303–306, doi: 10.1130/0091-7613(1991)019<0303:HAITLB>2.3.CO;2

Glasby G P, Iizasa K, Yuasa M, et al. 2000. Submarine hydrothermal mineralization on the Izu–bonin arc, south of Japan: an overview. Marine Georesources & Geotechnology, 18(2): 141–176

Glasby G P, Notsu K. 2003. Submarine hydrothermal mineralization in the Okinawa Trough, SW of Japan: an overview. Ore Geology Reviews, 23(3–4): 299–339

Grant H L J, Hannington M D, Petersen S, et al. 2018. Constraints on the behavior of trace elements in the actively-forming TAG deposit, Mid-Atlantic ridge, based on LA-ICP-MS analyses of pyrite. Chemical Geology, 498: 45–71, doi: 10.1016/j.chemgeo.2018.08.019

Hawkins Jr J W. 1995. The geology of the Lau Basin. In: Taylor B, ed. Backarc Basins: Tectonics and Magmatism. Boston: Springer, 63–138

Hein J R, de Ronde C E J, Koski R A, et al. 2014. Layered hydrothermal barite-sulfide mound field, East Diamante caldera, Mariana volcanic arc. Economic Geology, 109(8): 2179–2206, doi: 10.2113/econgeo.109.8.2179

Hongo Y, Nozaki Y. 2001. Rare earth element geochemistry of hydrothermal deposits and *Calyptogena* shell from the Iheya ridge vent field, Okinawa Trough. Geochemical Journal, 35(5): 347–354, doi: 10.2343/geochemj.35.347

James R H, Elderfield H. 1996. Chemistry of ore-forming fluids and mineral formation rates in an active hydrothermal sulfide deposit on the Mid-Atlantic Ridge. Geology, 24(12): 1147–1150, doi: 10.1130/0091-7613(1996)024<1147:COOFFA>2.3.CO;2

James R H, Green D R H, Stock M J, et al. 2014. Composition of hydrothermal fluids and mineralogy of associated chimney material on the East Scotia Ridge back-arc spreading centre. Geochimica et Cosmochimica Acta, 139: 47–71, doi: 10.1016/j.gca.2014.04.024

Karig D E. 1970. Ridges and basins of the Tonga-Kermadec island arc

system. Journal of Geophysical Research, 75(2): 239–254, doi: 10.1029/JB075i002p00239

Keith M, Haase K M, Schwarz-Schampera U, et al. 2014. Effects of temperature, sulfur, and oxygen fugacity on the composition of sphalerite from submarine hydrothermal vents. Geology, 42(8): 699–702, doi: 10.1130/G35655.1

Keith M, Häckel F, Haase K M, et al. 2016. Trace element systematics of pyrite from submarine hydrothermal vents. Ore Geology Reviews, 72: 728–745, doi: 10.1016/j.oregeorev.2015.07.012

Kim J, Son S K, Son J W, et al. 2009. Venting sites along the Fonualei and Northeast Lau Spreading Centers and evidence of hydrothermal activity at an off-axis caldera in the northeastern Lau Basin. Geochemical Journal, 43(1): 1–13, doi: 10.2343/geochemj.0.0164

Koski R A, Jonasson I R, Kadko D C, et al. 1994. Compositions, growth mechanisms, and temporal relations of hydrothermal sulfide-sulfate-silica chimneys at the northern Cleft segment, Juan de Fuca Ridge. Journal of Geophysical Research, 99(B3): 4813–4832, doi: 10.1029/93JB02871

Lehrmann B, Stobbs I J, Lusty P A J, et al. 2018. Insights into extinct seafloor massive sulfide mounds at the TAG, Mid-Atlantic ridge. Minerals, 8(7): 302, doi: 10.3390/min8070302

Lisitzin A P, Lukashin V N, Gordeev V V, et al. 1997. Hydrological and geochemical anomalies associated with hydrothermal activity in SW Pacific marginal and back-arc basins. Marine Geology, 142(1–4): 7–45

Malahoff A, Falloon T. 1991. Preliminary report of the RV *Akademik Mstislav Keldysh*/ MIR cruise 1990, Lau Basin Leg (May 7–21), on behalf of the Keldysh/ Mir Science Team. http://pacific-data.sprep.org/dataset/preliminary -report-akademik-mstislav-keldyshmir-cruise-1990-lau-basin-leg-may-7-21-1[2022-5-1]

Maslennikov V V, Cherkashov G, Artemyev D A, et al. 2020. Pyrite varieties at Pobeda hydrothermal fields, Mid-Atlantic ridge 17°07′–17°08′N: LA-ICP-MS data deciphering. Minerals, 10(7): 622, doi: 10.3390/min10070622

Maslennikov V V, Maslennikova S P, Large R R, et al. 2017. Chimneys in Paleozoic massive sulfide mounds of the Urals VMS deposits: mineral and trace element comparison with modern black, grey, white and clear smokers. Ore Geology Reviews, 85: 64–106, doi: 10.1016/j.oregeorev.2016.09.012

Meng Xingwei, Li Xiaohu, Chu Fengyou, et al. 2020. Trace element and sulfur isotope compositions for pyrite across the mineralization zones of a sulfide chimney from the East Pacific Rise (1–2°S). Ore Geology Reviews, 116: 103209, doi: 10.1016/j.oregeorev.2019.103209

Mills R A, Elderfield H. 1995. Rare earth element geochemistry of hydrothermal deposits from the active TAG mound, 26°N mid-Atlantic ridge. Geochimica et Cosmochimica Acta, 59(17): 3511–3524, doi: 10.1016/0016-7037(95)00224-N

Mottl M J, Seewald J S, Wheat C G, et al. 2011. Chemistry of hot springs along the Eastern Lau Spreading Center. Geochimica et Cosmochimica Acta, 75(4): 1013–1038, doi: 10.1016/j.gca.2010.12.008

Münch U, Blum N, Halbach P. 1999. Mineralogical and geochemical features of sulfide chimneys from the MESO zone, Central Indian Ridge. Chemical Geology, 155(1–2): 29–44

Münch U, Lalou C, Halbach P, et al. 2001. Relict hydrothermal events along the super-slow Southwest Indian spreading ridge near 63°56′E—mineralogy, chemistry and chronology of sulfide samples. Chemical Geology, 177(3–4): 341–349

Paropkari A L, Ray D, Balaram V, et al. 2010. Formation of hydrothermal deposits at Kings Triple Junction, northern Lau back-arc basin, SW Pacific: the geochemical perspectives. Journal of Asian Earth Sciences, 38(3–4): 121–130

Parson L M, Pearce J A, Murton B J, et al. 1990. Role of ridge jumps and ridge propagation in the tectonic evolution of the Lau back-arc basin, Southwest Pacific. Geology, 18(5): 470–473, doi: 10.1130/0091-7613(1990)018<0470:RORJAR>2.3.CO;2

Pearce J A, Ernewein M, Bloomer S H, et al. 1994. Geochemistry of Lau Basin volcanic rocks: influence of ridge segmentation and arc proximity. Geological Society, London, Special Publications, 81(1): 53–75

Perrin A, Goes S, Prytulak J, et al. 2018. Mantle wedge temperatures and their potential relation to volcanic arc location. Earth and Planetary Science Letters, 501: 67–77, doi: 10.1016/j.epsl.2018.08.011

Ray D, Banerjee R, Balakrishnan S, et al. 2017. S- and Sr-isotopic compositions in barite–silica chimney from the Franklin Seamount, Woodlark Basin, Papua New Guinea: constraints on genesis and temporal variability of hydrothermal fluid. International Journal of Earth Sciences, 106(5): 1723–1733, doi: 10.1007/s00531-016-1381-5

Ray D, Banerjee R, Mazumder A, et al. 2018. Mineralogical and geochemical variation in hydrothermal sulfides from Vienna Woods field, Manus Basin, Papua New Guinea: constraints on their evolution. Acta Oceanologica Sinica, 37(4): 22–33, doi: 10.1007/s13131-018-1194-4

Ray D, Kota D, Das P, et al. 2014. Microtexture and distribution of minerals in hydrothermal barite-silica chimney from the Franklin Seamount, SW Pacific: Constraints on mode of formation. Acta Geologica Sinica-English Edition, 88(1): 213–225, doi: 10.1111/1755-6724.12192

Scott S D. 1983. Chemical behaviour of sphalerite and arsenopyrite in hydrothermal and metamorphic environments. Mineralogical Magazine, 47(345): 427–435, doi: 10.1180/minmag.1983.047.345.03

Stoffers P, Worthington T J, Schwarz-Schampera U, et al. 2006. Submarine volcanoes and high-temperature hydrothermal venting on the Tonga arc, Southwest Pacific. Geology, 34(6): 453–456, doi: 10.1130/G22227.1

Sun Zhilei, Zhou Huaiyang, Yang Qunhui, et al. 2012. Growth model of a hydrothermal low-temperature Si-rich chimney: Example from the CDE hydrothermal field, Lau Basin. Science China Earth Sciences, 55(10): 1716–1730, doi: 10.1007/s11430-012-4485-1

Suzuki R, Ishibashi J I, Nakaseama M, et al. 2008. Diverse range of mineralization induced by phase separation of hydrothermal fluid: case study of the Yonaguni Knoll IV hydrothermal field in the Okinawa Trough back-arc basin. Resource Geology, 58(3): 267–288, doi: 10.1111/j.1751-3928.2008.00061.x

Tivey M K. 1995. The influence of hydrothermal fluid composition and advection rates on black smoker chimney mineralogy: insights from modeling transport and reaction. Geochimica et Cosmochimica Acta, 59(10): 1933–1949, doi: 10.1016/0016-7037(95)00118-2

Wang Shujie, Li Huaiming, Zhai Shikui, et al. 2017a. Geochemical features of sulfides from the deyin-1 hydrothermal field at the southern Mid-Atlantic ridge near 15°S. Journal of Ocean University of China, 16(6): 1043–1054, doi: 10.1007/s11802-017-3316-6

Wang Shujie, Li Huaiming, Zhai Shikui, et al. 2017b. Mineralogical characteristics of polymetallic sulfides from the Deyin-1 hydrothermal field near 15°S, southern Mid-Atlantic Ridge. Acta Oceanologica Sinica, 36(2): 22–34, doi: 10.1007/s13131-016-0961-3

Wohlgemuth-Ueberwasser C C, Viljoen F, Petersen S, et al. 2015. Distribution and solubility limits of trace elements in hydrothermal black smoker sulfides: an *in-situ* LA-ICP-MS study. Geochimica et Cosmochimica Acta, 159: 16–41, doi: 10.1016/j.gca.2015.03.020

Zellmer K E, Taylor B. 2001. A three-plate kinematic model for Lau basin opening. Geochemistry, Geophysics, Geosystems, 2(5): 2000GC000106

Zeng Zhigang, Ma Yao, Yin Xuebo, et al. 2015. Factors affecting the rare earth element compositions in massive sulfides from deep-sea hydrothermal systems. Geochemistry, Geophysics, Geosystems, 16(8): 2679–2693

Zhang Xia, Zhai Shikui, Yu Zenghui, et al. 2018. Mineralogy and geological significance of hydrothermal deposits from the Okinawa Trough. Journal of Marine Systems, 180: 124–131, doi: 10.1016/j.jmarsys.2016.11.007